ORIGINAL PAPER

Effect of temperature on synchronization of scale-free neuronal network

Yong Wu · Qianming Ding · Tianyu Li · Dong Yu · Ya Jia

Abstract The ambient temperature and the time delay of signal transmission are very important influences on the synchronization behavior of neuronal networks. In this paper, a neuronal network with the power-law degree distribution is constructed using a Hodgkin–Huxley model containing a temperature modulation factor and noise, and neurons at each node of the scale-free network are interconnected by electrical and chemical synapses, respectively. In scale-free networks with different ambient temperatures, the absence of time delay causes the synchronization of networks connected by both synaptic types to increase with coupling strength at lower temperatures, while the opposite is shown for networks connected by chemical synapses at higher temperatures. Networks connected by both synaptic types show multiple synchronization transitions when there is the time delay. Surprisingly, there is a temperature threshold for scale-free networks connected by chemical synapses, beyond which synchronization becomes very poor. By introducing the coefficient of variation and the mean inter-spikes intervals, it is found that the emergence of temperature thresholds for networks connected by chemical synapses is caused by a further increase in the difference in firing frequency of neurons due to increasing temperature. Finally, the

Y. Wu · Q. Ding · T. Li · D. Yu · Y. Jia (✉)
Department of Physics, Central China Normal University,
Wuhan 430079, China
e-mail: jiay@ccnu.edu.cn

generality of the results and mechanisms studied in scale-free networks is verified by investigating the effects of different network scales on synchronization.

1 Introduction

The nervous system is a typical nonlinear system, in which neuron is an extremely important specialized cell, and the research in neuroscience had been focused on the various dynamic properties of neuron. In 1952, Hodgkin and Huxley [1] established the famous Hodgkin–Huxley (HH) model based on experimental data of neuronal great axons in the squid, using the current balance formula and considering ion channel effects. Subsequently, the HH model has been widely studied in computational neuroscience because of its very good biological significance [2–4], and many derivative models [5–10] have been applied in different studies. The HH model has been widely used in various studies because it contains a temperature factor that allows it to accurately quantify much of the firing activity of neurons in different ambient temperatures. For example, Yu et al. [11] used the HH model to study neuronal responses to filtered signals. Ding et al. [12] investigated the effects

of temperature and ion channel blockage on myelinated axons composed of an improved HH model.

Neurons can communicate with each other due to the presence of an important site called a synapse, where information can be transmitted from one neuron to another [13–15]. The synapses can be roughly divided into electrical and chemical synapses due to the different ways of transmitting information. Electrical synapses allow continuous communication between neurons through gaps in the membrane, while chemical synapses transmit information to other neurons by releasing neurotransmitters [16]. These two types of synapses cause different electrical activity of neurons in the network, so it is extremely important to study networks with different synaptic connections. The effects and mechanisms of both types of synapses have been extensively studied [17, 18]. Andreev et al. [19] investigated the emergence of chimeric states in bistable HH in scale-free, small-world and random networks containing chemical synapses.

In computational neuroscience, a neuron is studied from the perspective of a multi-compartment model [20–22], which simulates a "real" neuron, and a single-compartment model [23–26], which abstracts the characteristics of the membrane potential. In networks composed of neurons, the transmission of action potentials in the network is usually studied, and to reduce the complexity of the network, the single-compartment model is mostly used [27–29]. To study the dynamics of neuronal populations in networks, many types of networks have been built, such as scale-free [30], small-world [31], and random networks [32]. Scale-free networks have been extensively studied because of their realistic features of growability and preferential connectivity [33–35]. Wang et al. [36] studied the effect of message transmission delay on synchronization in a scale-free network using Rulkov map. Hao et al. [37] investigated the difference between chemical and electrical synaptic effects on synchronization in a scale-free network.

Important phenomena such as synchronization occur when neurons in a neuronal network transmit information to each other [38–41] and they all have a very important role [42–46]. Synchronization phenomena have been discovered and carefully studied in living organisms [47, 48]. In neuroscience, it has been found in many studies that synchronization can occur both in good organismal behavior, such as processes of memory [49] and consciousness formation [50], cortical areas of visual motion [51], and problems of cognitive level [52], as well as in some organismal diseases, such as epilepsy [53] and parkinsonism [54]. Therefore, it is of great importance to study the synchronization behavior in complex networks, and much valuable work has been done in scale-free networks [55–57].

The HH model incorporates a temperature factor to accommodate experimental data at different temperatures [1, 58]. Temperature has been shown to be critical in many biological experiments as well as in computational simulations [59–61]. Temperature affects the activity of ion channels of neurons and the efficiency of energy transfers, and therefore can have a dramatic impact on the information propagation and collective dynamics of neural networks [62].

Signal transmission in the nervous system can be affected by some important intrinsic factors, such as noise [63–66] with time delay of signal transmission. In this paper, a Gaussian white noise with ideal statistical properties is used. Many biological experiments [67–69] have shown that action potentials propagate along axons at a speed of 20 to 60 m/s [70], so the time delay of signal transmission in the nervous system is widely present. Guo et al. [71] investigated the intrinsic coding mechanism of signals in neurons by adding Gaussian white noise to auditory neurons. Wang et al. [72] examined the effect of external electric fields on the synchronization of neuronal network systems in the presence of Gaussian white noise.

This paper focuses on the effect of ambient temperature and signal transmission delay on scale-free neural networks. Previous studies have shown the existence of an optimal temperature for signal transmission in the network [12], and we investigate the existence of a threshold for the effect of temperature on the network synchronization network and the possible mechanisms for its existence. The network undergoes multiple synchronization transitions under the influence of time delays [36], and we discuss the appearance of multiple synchronization transitions under the influence of temperature and the effect of time delays on it. The degree of nodes varies widely in scale-free networks [30], and we explore the robustness of multiple synchronization transitions under the influence of temperature at different network scales, showing the generality of the findings.

In this paper, a scale-free network composed of HH neuron models containing temperature modulators is employed. Neurons in the network are interconnected by electrical and chemical synapses, respectively, and their changes in membrane potential are interfered by white noise. A statistic called the synchronization factor is introduced to quantify the visually observed synchronization phenomenon and to explore the effect of ambient temperature and time delay on the synchronization of the network. To reveal the underlying mechanism in the phenomenon, the coefficient of variation (CV) and the mean inter-spikes intervals (ISIs) are used in the study.

2 Mathematical model and methods

For studying the dynamics of neurons in a network, the Hodgkin–Huxley (HH) model is used as the node of the network, which can describe the change of neuronal transmembrane potential with time. A Gaussian white noise is added to the spatio-temporal evolution of the neurons in the network to play a certain interference role. The mathematical model is described as follows:

$$\begin{cases} c_m \dfrac{dV_i}{dt} = -I_{i\mathrm{Na}} - I_{iK} - I_{iL} + I_{i\mathrm{ext}} + I_{i\mathrm{syn}} + \xi_i(t), \\ I_{i\mathrm{Na}} = g_{\mathrm{Na}} m_i^3 h_i (V_i - V_{\mathrm{Na}}), \\ I_{iK} = g_k n_i^4 (V_i - V_k), \\ I_{iL} = g_L (V_i - V_L), \end{cases}$$
(1)

where c_m describes the membrane capacitance per unit area of the neuron, which is fixed to $1\mu F/\mathrm{cm}^2$ in this study. V_i denotes the transmembrane potential of the i-th neuron in the network. The sequences of neurons of the network are all denoted in the equation by the subscript i ($i = 1,\ldots,N$; N is the total number of nodes in the network). The delayed-rectified K^+ channel current, the transient Na^+ channel current and the leakage current of HH model are denoted by $I_{i\mathrm{ext}}$, $I_{i\mathrm{Na}}$ and $I_{i\mathrm{L}}$, respectively. The maximum conductivities of the ion channels used in the model are g_{Na} = 120 mS/cm^2, g_K = 36 mS/cm^2 and g_L = 0.3mS/cm^2. The reversal potentials of the corresponding ion channels are V_{Na} = 50 mV, V_K = −77 mV and V_{L} = −54.4 mV, respectively. The detailed meaning of these parameters can be seen in [1]. $I_{i\mathrm{ext}}$ means the external electrode current per unit area of the injected

neurons. The Gaussian white noise added to the model is denoted by $\xi_i(t)$, and its statistical properties are the mean $\langle \xi_i(t) \rangle = 0$, and the autocorrelation $\langle \xi_i(t)\xi_i(t') \rangle = 2D\delta(t - t')$. $\delta(t)$ is the Dirac function, and D is the noise intensity and is fixed to 0.1 mA/cm^2. The three gating variables (n, m, h) in the model are denoted as follows:

$$\frac{\mathrm{d}x_i}{\mathrm{d}t} = \alpha_{x_i}(V_i)(1 - x_i) - \beta_{x_i}(V_i)x_i, \quad (x = n, m, h)$$
(2)

where the terms $\alpha_{x_i}(V_i)$ and $\beta_{x_i}(V_i)$ denote the opening and closing rates of the counterpart ion channels, respectively, and they are expressed as follows:

$$\begin{cases} \alpha_{n_i}(V_i) = \dfrac{0.01\phi(T)(V_i + 55)}{1 - \exp(-(V_i + 55)/10)}, \\ \beta_{n_i}(V_i) = 0.125\phi(T)\exp(-(V_i + 65)/80), \\ \alpha_{m_i}(V_i) = \dfrac{0.1\phi(T)(V_i + 40)}{1 - \exp(-(V_i + 40)/10)}, \\ \beta_{m_i}(V_i) = 4\phi(T)\exp(-(V_i + 40)/18), \\ \alpha_{h_i}(V_i) = 0.07\phi(T)\exp(-(V_i + 65)/20), \\ \beta_{h_i}(V_i) = \dfrac{\phi(T)}{1 + \exp(-(V_i + 35)/10)}. \end{cases}$$
(3)

In the above equations, m and h describe the degree of activation and inactivation of Na^+, respectively, while n indicates the activation of K^+. From the Law of Arrhenius, the effect of the ambient environment temperature to which the neuron is exposed can be obtained using the temperature modulation factor $\phi(T)$. In different species, this factor is different [58]. In this study, the values obtained in the experiments on the giant nerve fibers of the squid are used and the expressions are as follows [1]:

$$\phi(T) = 3^{(T-6.3\,^\circ\mathrm{C})/10\,^\circ\mathrm{C}}.$$
(4)

The term T means the temperature of environment. It has been shown in previous studies [73] that neurons begin to shift to a resting state at $T = 24\,^\circ$C. The temperature range studied in this paper is between $0\,^\circ$C and $24\,^\circ$C.

In this work, electrical and chemical synapses are used for the connection of neurons in the network, respectively. The electrical synapse can be expressed as:

$$I_{i\mathrm{syn}} = \sum_j G_{ij}\varepsilon_{ij}(V_j(t - \tau) - V(t)_i),$$
(5)

where G_{ij} are the coupling intensity. For simplicity, the coupling intensity between neurons is set to the

same value G in the study. ε_{ij} is the connection matrix, and τ is the delay in the transmission of synaptic signals. For chemical synaptic currents, the expression with α function can be as follows [74]:

$$\begin{cases} I_{i\text{syn}} = \sum_j G_{ij}\varepsilon_{ij}\alpha(t - \tau - t_j)(V_{\text{syn}} - V_i), \\ \alpha(t) = \dfrac{t}{\tau_{\text{syn}}}\exp(-\dfrac{t}{\tau_{\text{syn}}})\Theta(t). \end{cases} \quad (6)$$

Same as the electrical synaptic current, G_{ij}, ε_{ij} and τ denote the coupling intensity, the connection matrix and time delay, respectively. t_j represents the last firing time of the j-th neuron before time $t - \tau$. V_{syn} is the synaptic reversal potential, which is used in the study for excitatory synapses, so it is set to 0 mV. The characteristic time constant for the interaction of two neurons τ_{syn} is fixed as 2 ms. $\Theta(t)$ is the Heaviside function.

The topology of the network has a significant effect on the transfer of information between neurons. This study uses the topology proposed by Barabási and Albert [30] called scale-free network, which has the property of growth and preferential connectivity. Unless noted otherwise, the number of nodes in the network is set to $N = 200$. Each node in the network is consistent with the neuronal oscillator in Eq. (1) and the connections between the nodes are represented by the connection matrix ε_{ij}. Based on Ref. [30], a new node is added to the network and the probability of connection to the old node is $p(k_i) = k_i \big/ \sum_j k_j$, where k_i denotes the degree of the i-th neuron. The initial number of nodes in the network is given as $m_0 = 5$, and they are interconnected. After that each new addition of nodes will be connected to two old nodes. The obtained network is the power-law degree distribution, which is on the double logarithmic graph with a slope of the line of about -3. This scheme of preferential connectivity and growth results in an average degree of $\langle k \rangle = \sum_i k_i / N = 4$ for the network in this work.

To quantify the synchronization of the network as observed visually, a statistical physical quantity called the synchronization factor is introduced into this study. This statistical physical quantity is based on mean-field theory and is defined as [75]:

$$R = \frac{\langle F^2 \rangle - \langle F \rangle^2}{\frac{1}{N}\sum_{i=1}^{N}\left(\langle V_i^2 \rangle - \langle V_i \rangle^2\right)}, \quad F = \frac{1}{N}\sum_{i=1}^{N} V_i. \quad (7)$$

The results of its calculation give a very good indicator of the condition of spatio-temporal synchronization of neurons in the network. By studying the synchronization factors under different conditions, the synchronization levels and synchronization transition of the network are revealed intuitively. The V_i in Eq. (7) is the transmembrane potential calculated from Eq. (1). N is the total number of neurons in the scale-free network. The term $\langle * \rangle$ denotes the temporal average of the variable over time. The synchronization factor R indicates the perfect and no synchronization by tending to 1 and 0, respectively.

3 Results and discussions

In this section, to obtain the numerical simulation results of the neuronal model in different cases, the Euler forward algorithm is used, and the step size is set to 0.01 ms. The transients caused by the initial values are removed before each calculation. In this study, the synchronization of neuron populations in the scale-free network is explored, so a suitable external electrode current is first selected. The external electrode current $I_{i\text{ext}} = 20\mu A/\text{cm}^2$ is chosen so that the neurons can generate spiking discharges. The space–time firing raster plots of the neuronal network are first investigated under different coupling intensities without considering the signal transmission delay ($\tau = 0$). In the spatiotemporal firing raster plots, the black dots indicate neuronal firing, while the white parts indicate the subthreshold values of neuronal membrane potentials. In Fig. 1, the spatiotemporal firing raster plots of the scale-free neuronal network connected by electrical synapses at different temperatures and at different coupling intensities are shown. The spatiotemporal firing raster plots with increasing coupling intensity are shown in the results of Fig. 1 for each of the two temperatures ($T = 0\,°C$ and $T = 10\,°C$). The results are a visual representation of the gradual increase in synchronization. Next, the spatiotemporal firing raster plots of the network connected by chemical synapses are investigated. The collective firing behavior of neurons at different temperatures ($T = 0\,°C$ and $T = 10\,°C$) with increasing coupling intensity is shown in Fig. 2.

A surprising phenomenon appears in Fig. 2, where the synchronization visually becomes better with
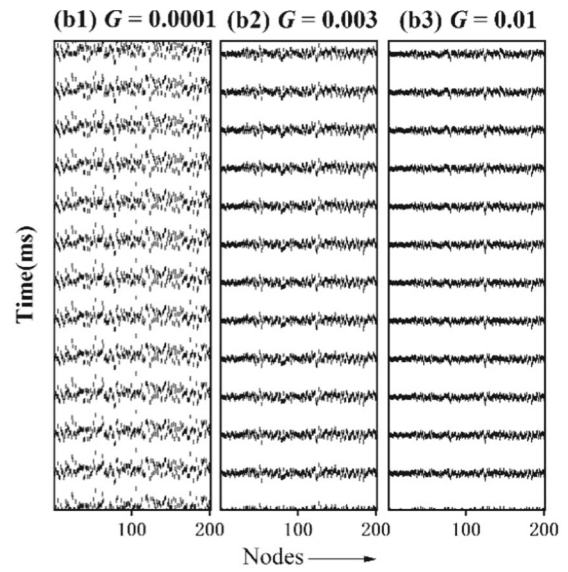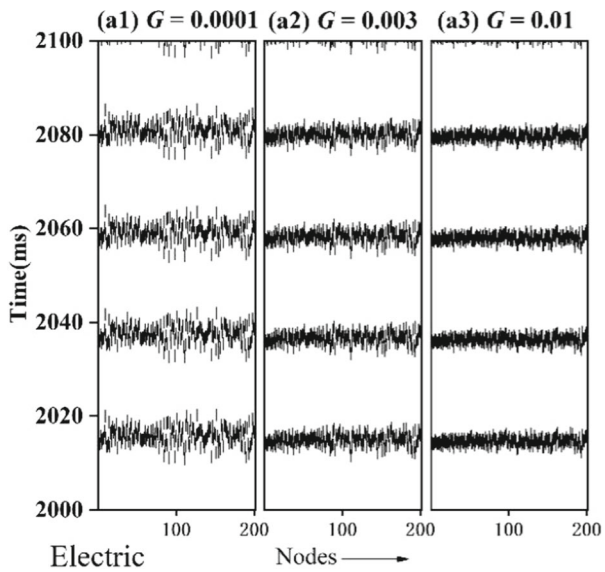
Fig. 1 Space–time firing raster plots of neuronal membrane potentials at different electrical synaptic coupling intensities G. Without considering the signal transmission delay ($\tau = 0$), the coupling intensity in the figure is **a1**, **b1** G = 0.0001; **a2**, **b2** G = 0.003; **a3**, **b3** G = 0.01 for temperature $T = 0\,^\circ$C and $T = 10\,^\circ$C. The synchronization becomes better as the coupling intensity increases
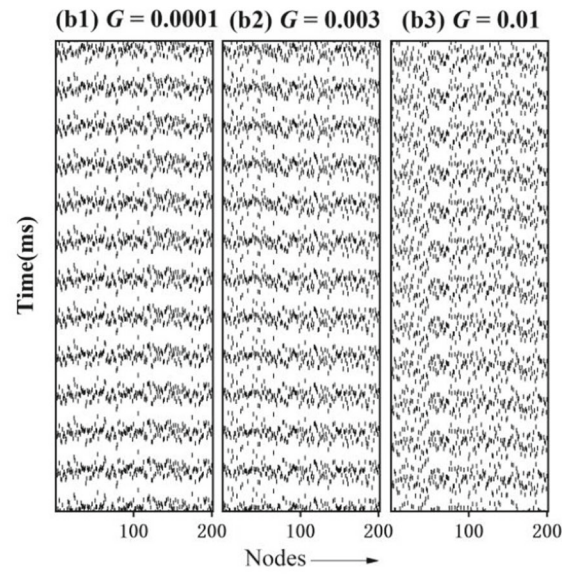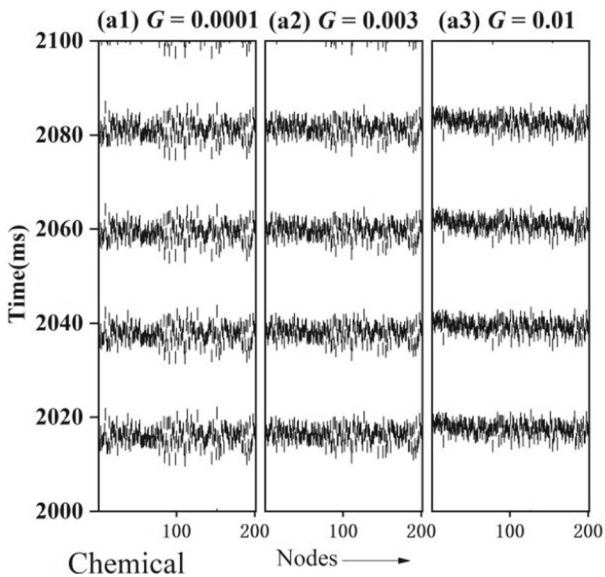
Fig. 2 Space–time firing raster plots of neuronal membrane potentials at different chemical synaptic coupling intensities G. Without considering the signal transmission delay ($\tau = 0$), the coupling intensity in the figure is **a1**, **b1** G = 0.0001; **a2**, **b2** G = 0.003; **a3**, **b3** G = 0.01 for temperature $T = 0\,^\circ$C and $T = 10\,^\circ$C. At larger temperatures, the synchronization becomes worse instead as the coupling intensity becomes larger

increasing coupling intensity at smaller temperatures, as in Fig. 2(a1, a2, and a3). However, at larger temperatures, the synchronization visually becomes worse with increasing coupling intensity, as in

Fig. 2(b1, b2, and b3). To quantify the visually observed synchronization phenomenon, synchronization factors are employed in the study. Next, the synchronization factors of the network connected by

electrical and chemical synapses with enhanced coupling intensity at different temperatures are shown in Fig. 3.

The results shown in Fig. 3 are consistent with the visual results in Figs. 1 and 2. The results in Fig. 3 indicate that the synchronization factor increases with increasing coupling intensity when the network is connected by electrical synapses. When the network is connected by chemical synapses, the synchronization factor increases with increasing coupling intensity for smaller temperatures and decreases with increasing coupling intensity for larger temperatures. The synchronization factor of the network connected by both electrical and chemical synapses decreases with increasing temperature at the same coupling intensity. The above results are further verified in Fig. 3(a2, b2) where

the coupling intensity G is further increased. The results clearly indicate that the synchronization factor of the network connected by chemical synapses decreases much more with increasing temperature than that of the network connected by electrical synapses. For a more comprehensive study of the dynamic behavior of the coupling intensity in different cases, the two-parameter diagrams of the synchronization factors of the coupling intensity G versus the time delay τ are shown in Fig. 4(a1, b1) when the ambient temperature is set to $T = 6.3$ °C. In the absence of time delay ($\tau = 0$), the two-parameter diagrams of the synchronization factors of the coupling intensity G versus the ambient temperature T are shown in Fig. 4(a2, b2).

The results in Fig. 4(a2, b2) show that, in the absence of time delay ($\tau = 0$), the synchronization of
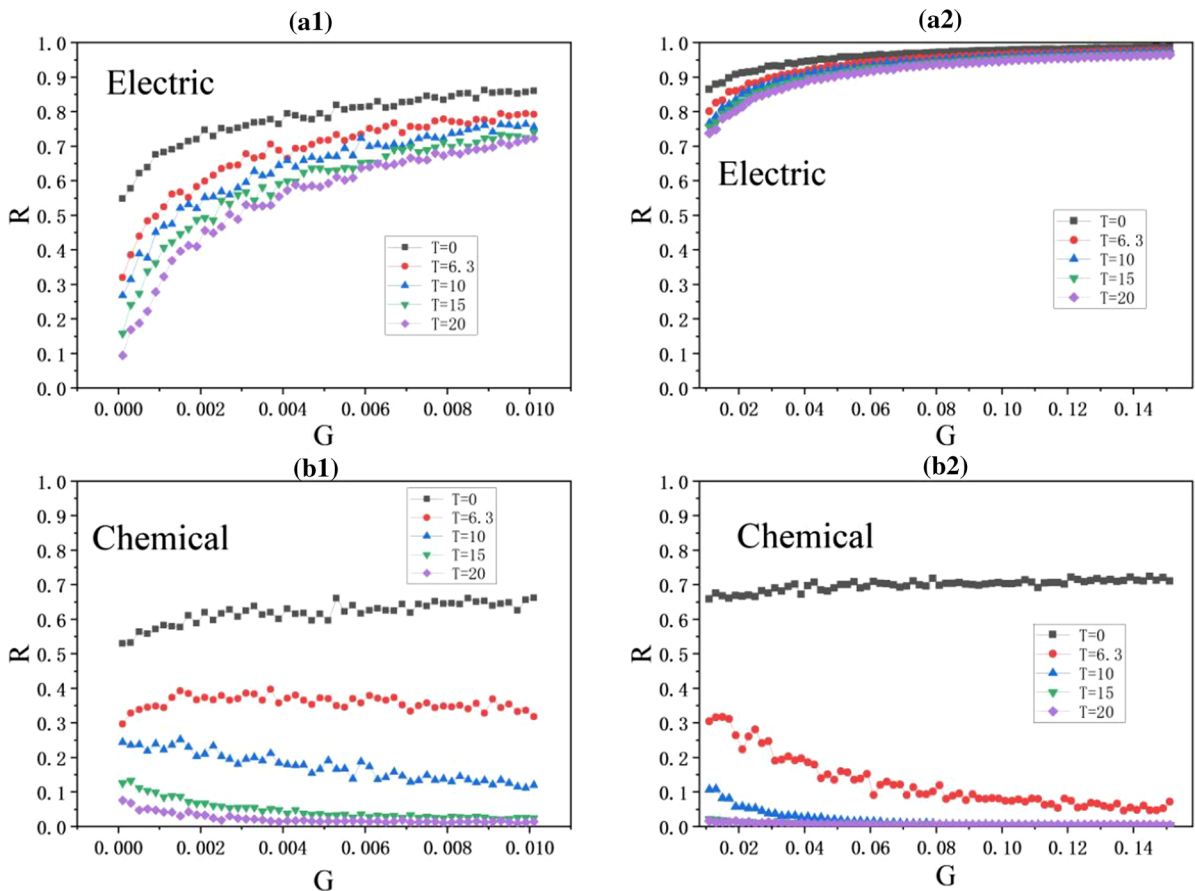
Fig. 3 Distribution of the synchronization factor with increasing coupling intensity G at different temperatures T. Without considering the signal transmission delay ($\tau = 0$), the synchronization factors of the network connected by electrical and chemical synapses are distributed in **a1**, **a2** and **b1**, **b2**,

respectively. When the coupling intensity increases, the synchronization factor of the network is enhanced for electrical synaptic connections, while that for chemical synaptic connections decreases at higher temperatures
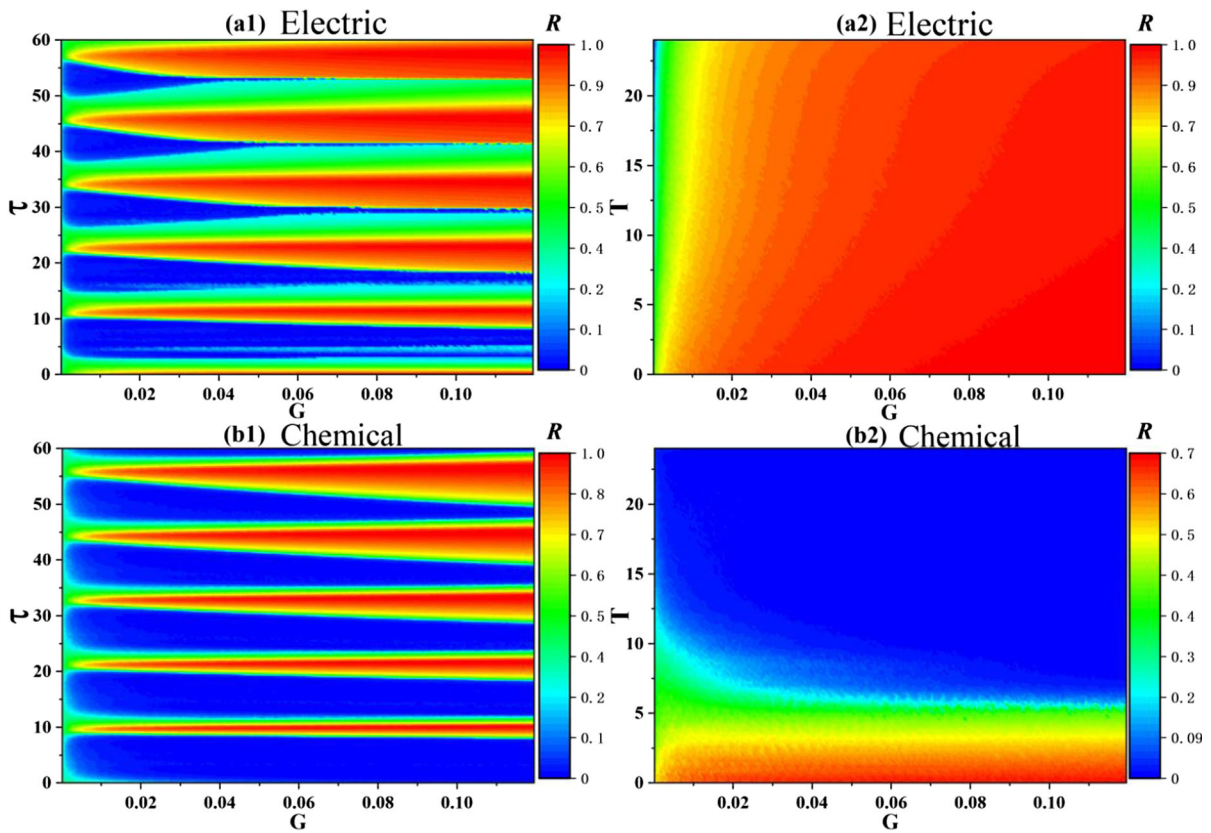
Fig. 4 Two-parameter diagram on the synchronization factor. The synchronization factors of the network connected by electrical and chemical synapses are distributed in **a1**, **b1** and **a2**, **b2**, respectively. (**a1**), (**b1**) The horizontal and vertical coordinates indicate the coupling intensity G and time delay τ of the network, respectively, and the ambient temperature is fixed at $T = 6.3$ °C. (**a2**), (**b2**) The horizontal and vertical coordinates indicate the coupling intensity G and the ambient temperature T of the network, respectively, and the time delay is fixed at $\tau = 0$

the network with increasing coupling intensity G at different temperatures T appears in perfect accordance with the results shown in Fig. 3. However, a temperature threshold emerges for the network connected by chemical synapses, such that the synchronization becomes very poor when it is greater than the threshold. The results in Fig. 4(a1, b1) show that the networks connected by electrical and chemical synapses show synchronous transitions with increasing time delays τ for different coupling intensities G. Considering that the signal processing and transmission in a real neural system takes a certain amount of time, a time delay τ will be added in the next study. In order to keep the system in a steady state for the next study, the synaptic coupling intensity will be fixed at $G = 0.1$. With the time delay set at $\tau = 30$ ms, the

spatiotemporal firing raster plots of the network connected by electrical and chemical synapses at different temperatures are shown in Fig. 5.

The results in Fig. 5 show that the networks connected by electrical and chemical synapses exhibit multiple synchronous transitions at different temperatures. Figure 5(a1), (a3) and (b1), (b3) shows very poor synchronization, while Fig. 5(a2), (a4) and (b2), (b4) shows very good synchronization. The results clearly show multiple transformations of synchronization, i.e., alternating from poor to good and back to poor transformations. Next, to investigate the effect of time delay, the temperature is set to $T = 5.3$ °C and the spatiotemporal firing raster plots at different time delays are displayed in Fig. 6. Similar to the results in Fig. 5, multiple synchronization transitions are also
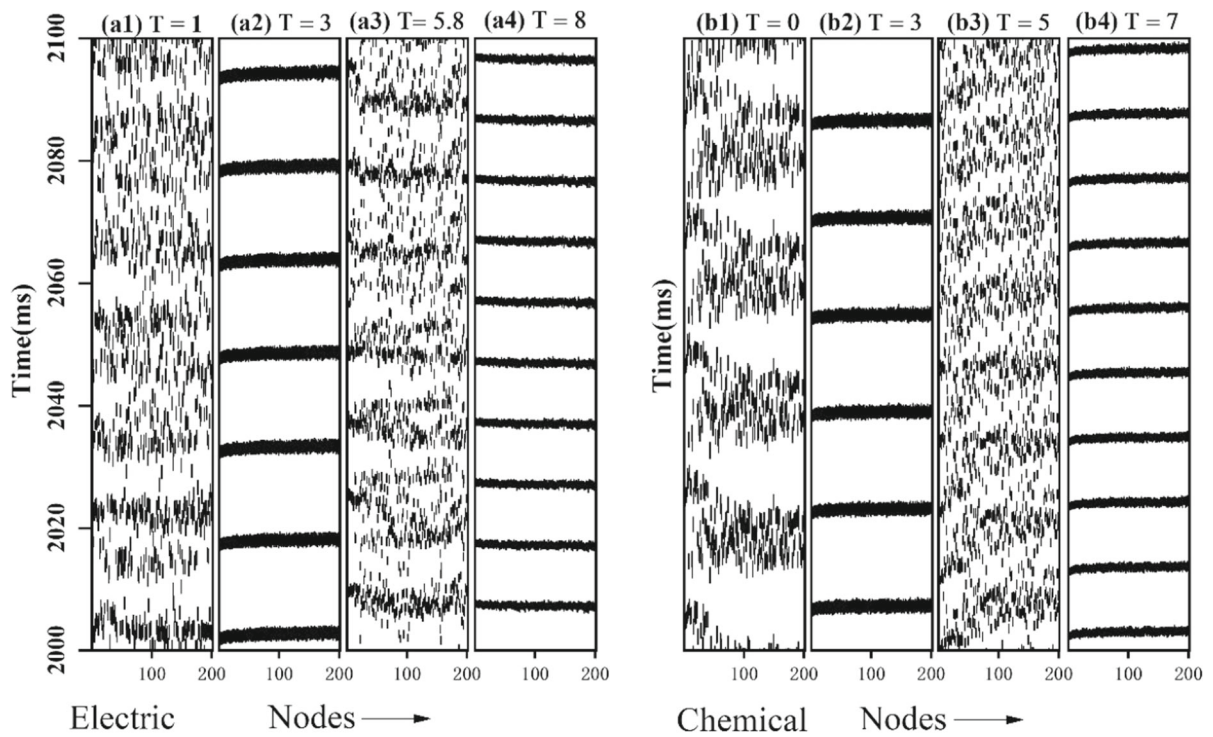
Fig. 5 Space–time firing raster plots of neuronal membrane potentials of the network connected by electrical and chemical synapses at different temperatures T. At the time delay of $\tau = 30$ ms and a coupling intensity of $G = 0.1$, the results of synchr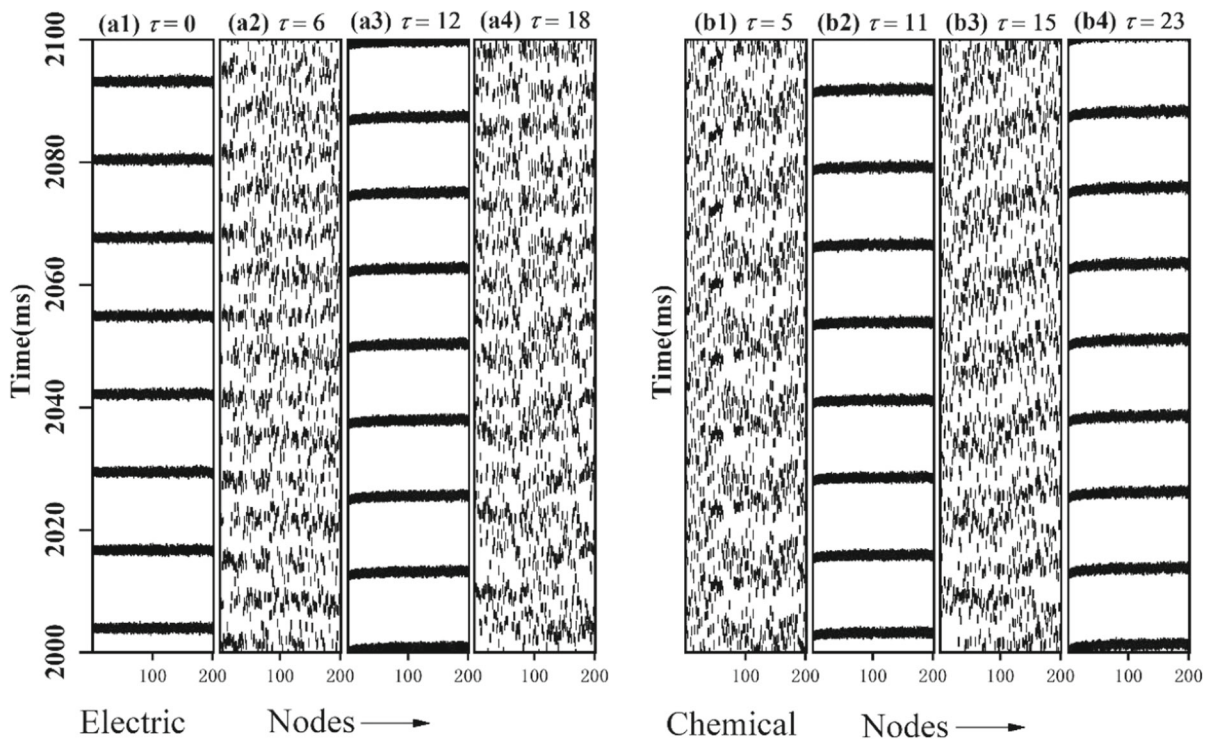onization of networks connected by electrical synapses at different ambient temperatures are shown for **a1**, **a2**, **a3**, **a4**, and of networks connected by chemical synapses for **b1**, **b2**, **b3**, **b4**, respectively. Both connection types showed multiple synchronization transitions at different temperatures

exhibited in Fig. 6 at different time delays. To observe this synchronization transition phenomenon more intuitively, the synchronization of the network is quantified using a synchronization factor. The distribution of the synchronization factor with increasing temperature at different time delays is illustrated in Fig. 7, and the distribution of the synchronization factor with increasing time delays at different temperatures is presented in Fig. 8.

The results in Fig. 7 show that at time delay of $\tau = 0$, as in Fig. 7(a1) and (b1), the synchronization factor of the network connected by electrical synapses is large and decreases only slightly with increasing temperature, which is consistent with the results in Fig. 3(a1) and (a2). The synchronization factor of the network connected by chemical synapses becomes smaller rapidly with increasing temperature, which is consistent with the results in Fig. 3(b1) and (b2). In the presence of suitable time delays, as in Fig. 7(a2), (a3)

and (b2), (b3), multiple synchronization transitions can be observed. Surprisingly, the results in Fig. 7 also show that when the network is connected by electrical synapses, the synchronization factor becomes larger overall as the temperature rises. When the network is connected by chemical synapses, the synchronization factor becomes very small when the temperature exceeds a threshold (approximately $T = 15\ °C$) and does not get larger afterward. The results in Fig. 8 indicate that the network connected by electrical synapses shows multiple synchronization transitions with increasing time delays at different temperatures and the synchronization factor becomes larger overall. The distribution of the synchronization factor of the network connected by chemical synapses also shows multiple synchronization transitions and an overall increase at lower temperatures, as in Fig. 8(b1). At higher temperatures, there are also multiple synchronization transitions and the overall is smaller, as in
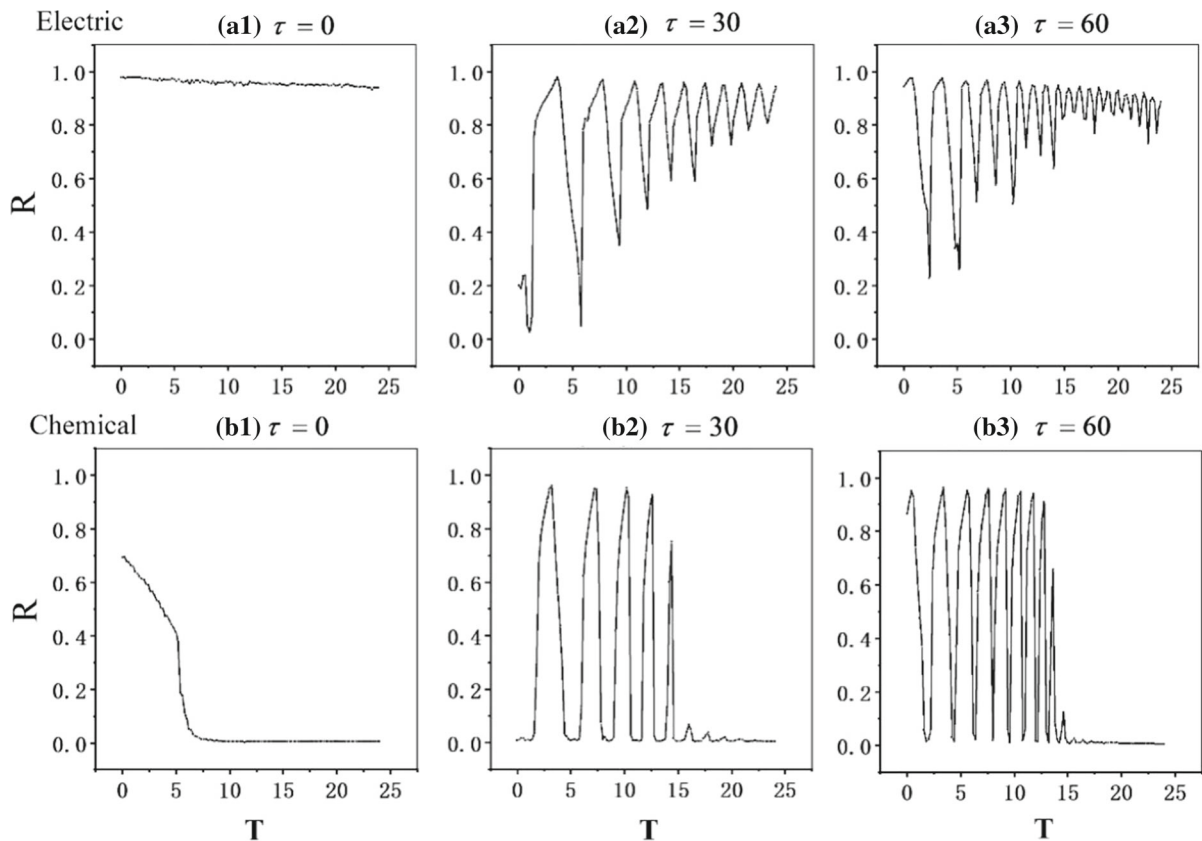
Fig. 6 Space–time firing raster plots of neuronal membrane potentials of the network connected by electrical and chemical synapses at different time delay τ. At the ambient temperature of $T = 5.3\ °C$ and a coupling intensity of $G = 0.1$, the results of synchronization of networks connected by electrical synapses at different time delay are shown for **a1**, **a2**, **a3**, **a4**, and of networks connected by chemical synapses for **b1**, **b2**, **b3**, **b4**, respectively. Both connection types showed multiple synchronization transitions at different temperatures

Fig. 8(b2). After the temperature exceeds the threshold, the synchronization factors become very small and do not get larger, as in Fig. 8(b3). To further investigate the multiple synchronization transitions of the network with respect to ambient temperature T and time delay τ, the two-parameter diagrams of the synchronization factors are plotted in Fig. 9.

The results in Fig. 9 show very clearly that the network connected by electrical and chemical synapses undergoes multiple synchronization transitions with increasing ambient temperature T and time delay τ. The time delay τ plays a crucial role for the synchronization transition. Both (a) and (b) of Fig. 9 show that when the time delay τ is relatively small, both decrease with increasing temperature and do not show multiple synchronization transitions. Networks connected by chemical synapses quickly become very poorly synchronized with increasing temperature when the time delay is small. With increasing time delay both networks undergo multiple synchronization transitions. Multiple synchronization transitions also

occur as the temperature increases under the effect of time delay. Figure 9 verifies the phenomenon found in Figs.7 and 8. The network, connected by electrical synapses, shows multiple synchronization transitions with increasing temperature under time delay, and its synchronization factor becomes larger overall. At larger time delays and temperatures, its synchronization becomes very good and does not become poor again, as shown in Fig. 9(a). For networks connected by chemical synapses, multiple synchronization transitions can occur at both increasing time delays and temperatures, while there exists a threshold value (approximately $T = 15\ °C$) for temperature beyond which the synchronization factor becomes very small and does not increase again, which is consistent with previous findings. It is further investigated that this previously observed phenomenon in which the synchronization factor of the network connected by electrical synapses becomes large at higher temperatures, and the synchronization factor of the network connected by chemical synapses becomes very small
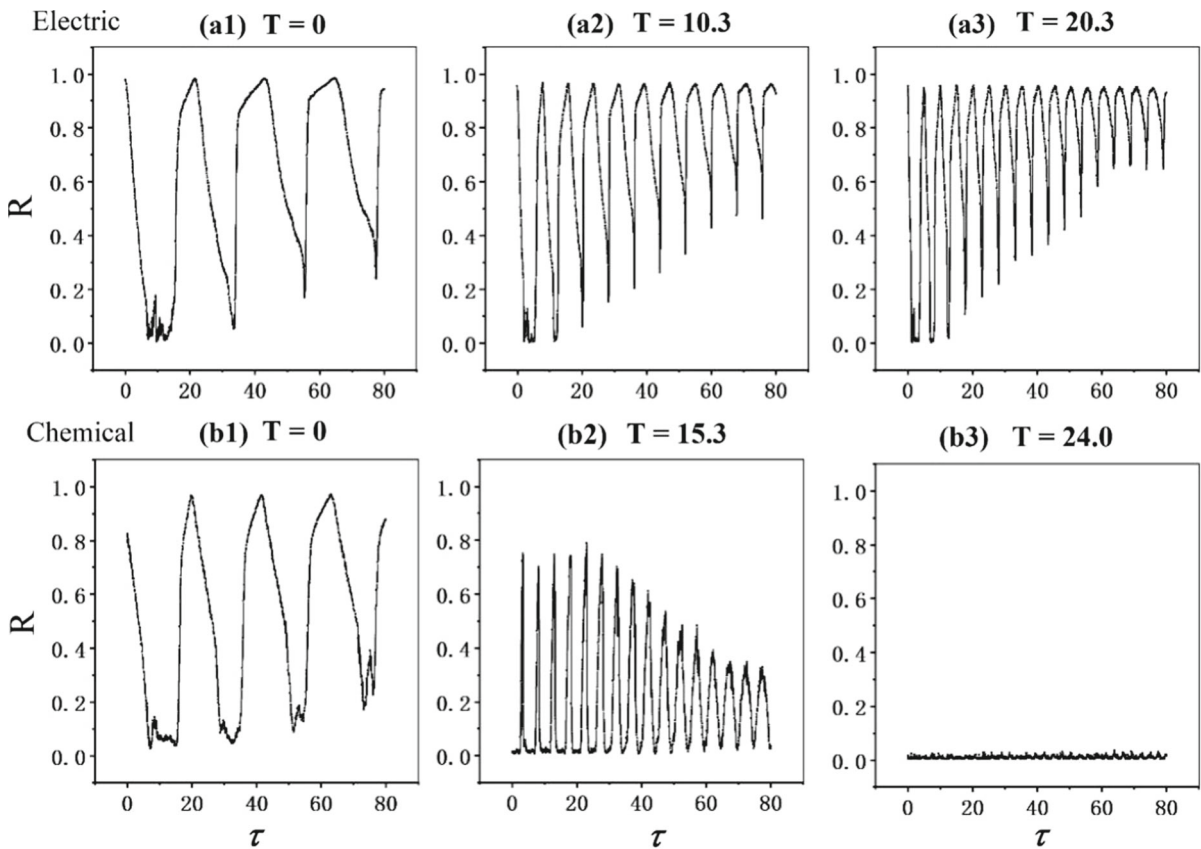
Fig. 7 Distribution of the synchronization factor with increasing ambient temperature T at different time delays τ. At the coupling intensity of $G = 0.1$, the results of the synchronization factor distribution of the network connected by electrical synapses are shown in **a1**, **a2**, **a3**, and of the network connected by chemical synapses are shown in **b1**, **b2**, **b3**. With a suitable time delay, multiple synchronization transitions are observed for both connection types

when the threshold is exceeded. The membrane potentials of the network at different temperatures for both types of connections (sampled neurons $i = 2$ and $i = 100$) are shown in Figs. 10 and 11.

Figures 10 and 11 show the membrane potential of neurons in the network connected by electrical and chemical synapses at a time delay of. In Fig. 10, it is shown that the firing frequency of neurons increases as the temperature T increases. There is a marked phase difference in Fig. 10(a) and (b), and this phase difference remains stable, which causes the asynchronization of the network. Figure 10(c) and (d) has a very small phase difference and the network is remarkably well synchronized, all of which are the same as the results shown in Fig. 7. It is assumed here

that the asynchronization of the network connected by electrical synapses is mainly due to the phase difference. When the temperature is too high, the neuronal firing frequency becomes larger, and the effect of phase difference on synchronization decreases as the firing frequency of neurons becomes larger. The asynchronization of the network connected by chemical synapses when the temperature is small is also shown in Fig. 11 mainly due to phase differences, as in (a) and (b). In Fig. 11(c) and (d), it is shown that the phase difference of the spikes changes from large to small and then to large again for larger temperatures in a cyclic process that causes the network asynchronization. It is assumed here that the reason for the asynchronization of the network connected by

Fig. 8 Distribution of the synchronization factor with increasing time delays τ at different ambient temperature T. At the coupling intensity of $G = 0.1$, the results of the synchronization 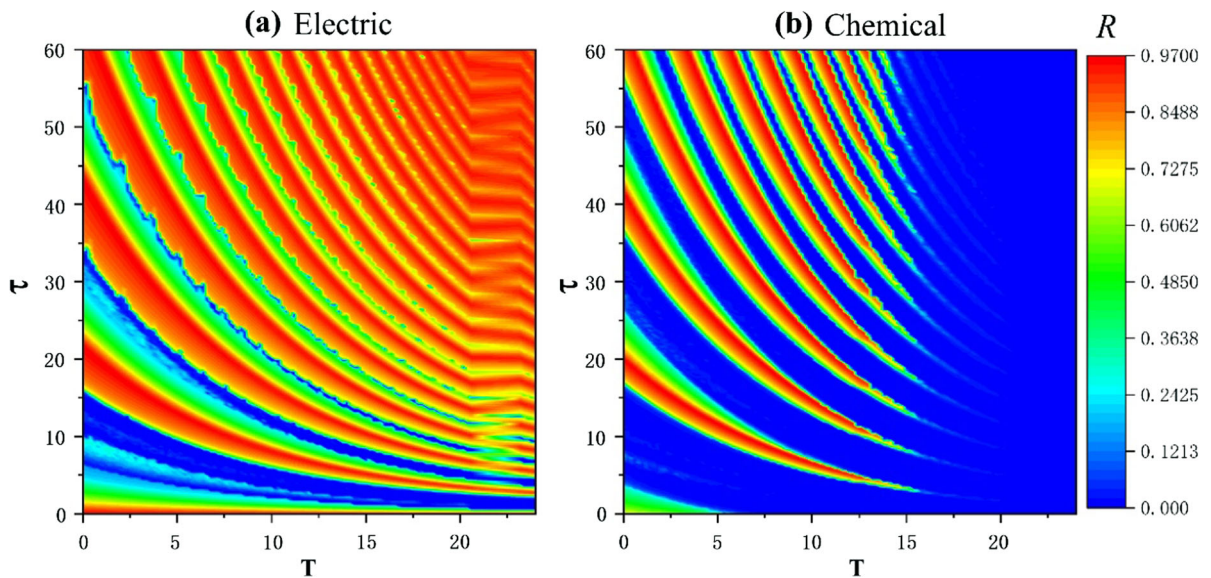factor distribution of the network connected by electrical synapses are shown in **a1**, **a2**, **a3**, and of the network connected by chemical synapses are shown in **b1**, **b2**, **b3**. As the time delay increases, multiple synchronization transitions are observed for both connection types

chemical synapses at temperatures above the threshold is mainly due to the inconsistent firing frequency of the neurons in the network. To verify the assumptions of studies that the synchronization of networks connected by electrical and chemical synapses becomes better and worse, respectively, when the temperature is too high, a statistic called the coefficient of variation (CV) and which systematically measures the degree of regularity of the neuronal electrical activity [76] is introduced, with the expression as follows:

$$CV_i = \frac{\sqrt{\langle ISI_i^2 \rangle - \langle ISI_i \rangle^2}}{\langle ISI_i \rangle} \tag{8}$$

where i denotes the i-th neuron in the neuronal network. $\langle ISI_i \rangle$ is the average of all inter-spikes intervals (ISIs) of the i-th neuron at a certain time. The firing of the i-th neuron becomes more regular as CV_i decreases. $\langle ISI_i \rangle$ is described as follows:

$$\langle ISI_i \rangle = \frac{1}{n} \sum_{j=1}^{n} (t_{j+1} - t_j) \tag{9}$$

Fig. 9 Two-parameter diagram on the synchronization factor with respect to ambient temperature T and time delay τ. At the coupling intensity of $G = 0.1$, the synchronization factors of the network connected by electrical and chemical synapses are distributed in **a** and **b**, respectively. The network connected by both connection types clearly shows multiple synchronization transitions

where t_j denotes the j-th spike of the i-th neuron, while n denotes the number of spikes. The duration of each calculation of the average ISI_i is 10,000 time units to ensure the statistical correctness.

In Fig. 12, (a1) and (b1) show the distribution of the CV of the network connected by electrical and chemical synapses, respectively, with increasing temperature at higher temperatures. The results show that the CVs of the 2-th and 100-th neurons of the network connected by both types and the average CV of the network are smaller. The smaller CVs indicate a better firing regularity of the network. As the temperature increases, the discharge frequency increases and the CV becomes smaller overall. The CV in Fig. 12(a1) will have regions that suddenly increase and then become smaller, and a comparison with Fig. 7(a2) reveals that these are the regions where the synchronization factor becomes smaller. This shows that the reduction in the network synchronization factor caused by phase asynchronization also makes the neuronal firing in the network connected by electrical synapses less regular, i.e., the CV becomes larger. The average ISI of the 2-th and 100-th neurons in the network connected by the two types and their differences are shown in (a2) and (b2). The results show that the average ISI decreases further with increasing temperature. Figure 12(a2) shows that the difference in the average ISI is very small almost close to zero. Combined with the conclusion of the large degree of network discharge regularity in (a1), this further supports the previous conclusion that the asynchronization of the network connected by the electrical synapses is due to the phase inconsistency of the spike firing, and that the effect of the phase inconsistency on synchronization decreases as the temperature increases and the frequency of the firing increases. The difference in the average ISI in Fig. 12(b2) is around 0.16, which indicates a difference of one spike for about 20 to 30 spikes. Combined with the conclusion of the large degree of network firing regularity in (b1), this further supports the previous conclusion that the asynchrony of networks connected by chemical synapses is a result of inconsistent firing frequency of neurons in the network, and the effect of inconsistent firing frequency on synchronization becomes larger as the temperature increases and the firing frequency becomes higher. Figure 12 illustrates very well the conclusion obtained in Fig. 11.
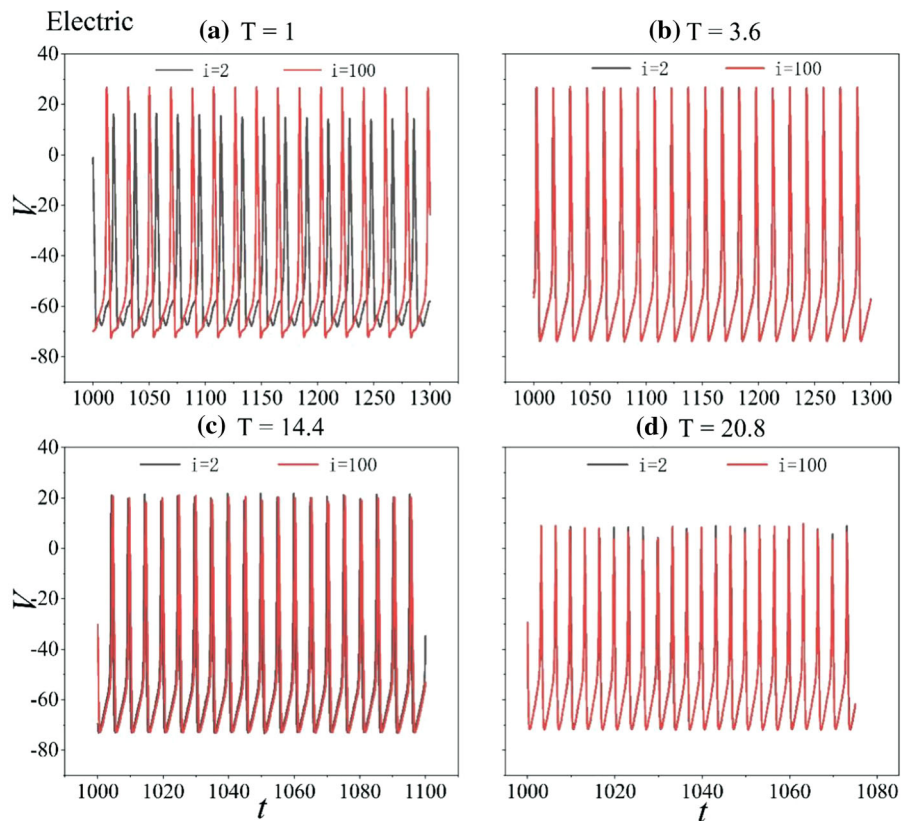
Fig. 10 Membrane potential of neurons ($i = 2$ and $i = 100$) in networks connected by electrical synapses. The time delay and the coupling intensity are fixed at $\tau = 30$ ms and $G = 0.1$, respectively. The membrane potentials of neurons at different temperatures are shown in **a**, **b**, **c**, and **d**, respectively. The asynchrony of the network connected by electrical synapses is caused by phase differences

To further verify the generality of the above study, the scale of the network, i.e., the number of nodes in the network, is changed to observe the effect on the distribution of synchronization factors and the results are shown in Fig. 13. The distribution of synchronization factors with increasing temperature for networks connected by both synaptic types at different network scales is shown in Fig. 13. The time delay is set at $\tau = 20$ ms, and the coupling strength is fixed at $G = 0.1$, and the number of nodes in the network is set to $N = 200, 400, 1000$ and 2000, respectively. The results in Fig. 13 show that changing the scale of the network has a very small and negligible effect on the network connected by the two synapse types. Such results further demonstrate the generality of the above study in the scale-free network.

4 Conclusions

In conclusion, the synchronization of neuron populations in scale-free networks is investigated at different ambient temperatures as well as time delays. The Hodgkin–Huxley (HH) model containing the temperature factor is employed as the model of neurons in the scale-free network for the study, and electrical and chemical synapses are used to connect the neurons, respectively. The synchronization factor is used to quantify the synchronization phenomenon observed visually in the network. It is found that networks connected by electrical and chemical synapses undergo synchronization transitions at different time delays and ambient temperatures. A temperature threshold is found in the network connected by

Fig. 11 Membrane potential of neurons ($i = 2$ and $i = 100$) in networks connected by chemical synapses. The time delay and the coupling intensity are fixed at $\tau = 30$ *ms* and $G = 0.1$, respectively. The membrane potentials of neurons at different temperatures are shown in **a**, **b**, **c**, and **d**, respectively. At higher temperatures, the asynchrony is caused by the different firing frequencies of the neurons in the network
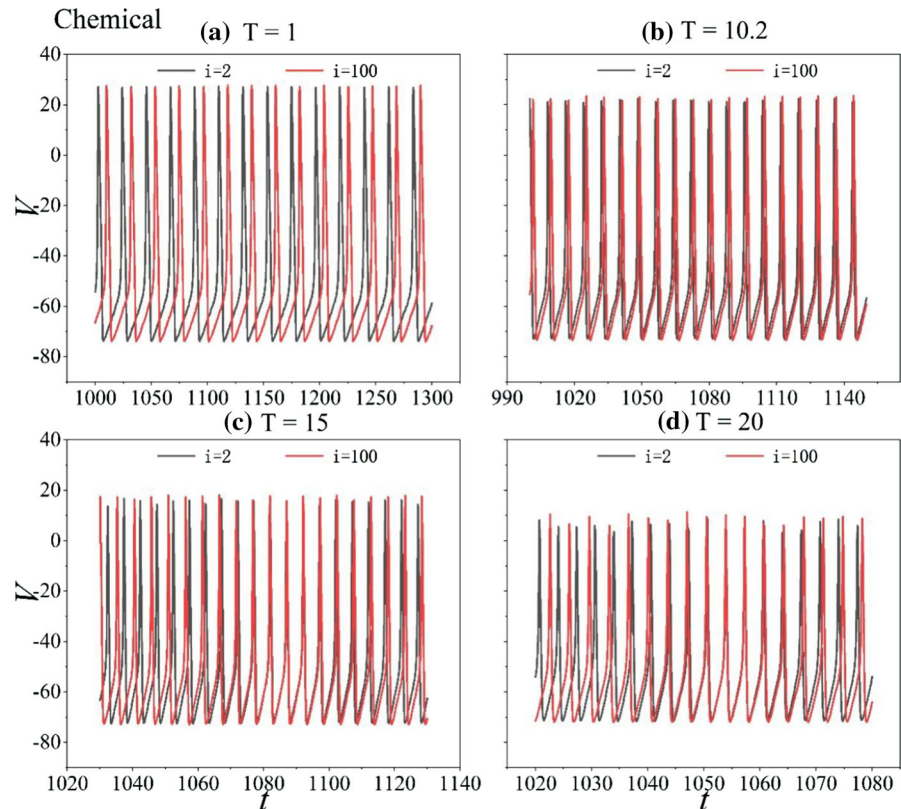

chemical synapses, beyond which the synchronization of the network becomes very poor.

Without considering the time delay, for networks connected by electrical synapses, the synchronization of the network becomes better as the coupling intensity increases. For networks connected by chemical synapses, as the coupling intensity increases, the network synchronization becomes better at lower temperatures, while at higher temperatures, the synchronization becomes worse instead. When the coupling intensity of the network is constant, the synchronization of the network connected by both synapses deteriorates with increasing temperature, while the deterioration is greater for the network connected by chemical synapses.

The network connected by the two synaptic types under consideration of time delay shows multiple synchronization transitions with increasing delay, and the network also shows multiple synchronization transitions with increasing temperature under the effect of time delay. At higher temperatures, the synchronization of the network connected by electrical synapses is better overall, while the synchronization of the network connected by chemical synapses turns very poor after the temperature exceeds a threshold (approximately $T = 15\ ^{\circ}$C) and does not get better again. By introducing the coefficient of variation (CV) as well as the mean inter-spikes intervals (ISIs), it turns out that the main reasons for this phenomenon at higher temperatures are: (1) In networks connected by electrical synapses, the main cause of asynchronization is the phase inconsistency of the neuronal spike firing. When the temperature increases, the firing frequency increases, which leads to an overall better synchronization of the network connected by electrical synapses at high temperatures. (2) In networks connected by chemical synapses, the main factor causing asynchronization is the inconsistent frequency (or average ISI) of neuronal spike firing. The increase in temperature makes the firing frequency increase, resulting in a phase difference of one spike for 20 to 30 spikes, and such a phenomenon causes a very poor synchronization of the network.

Fig. 12 Coefficient of variation (CV) and mean inter-spikes intervals (ISIs) with respect to temperature for the 2-th and 100-th neurons of the network connected by electrical and chemical synapses at higher temperatures. The time delay and the coupling intensity are fixed at $\tau = 30\ ms$ and $G = 0.1$, respectively. **a1**, **b1** Distribution of the CV of the 2-th and 100-th neurons and the average CV of all neurons in the neuronal network as the temperature increases; **a2**, **b2** Distribution of the average ISI of the 2-th and 100-th neurons and the difference as the temperature increases in the neuronal network
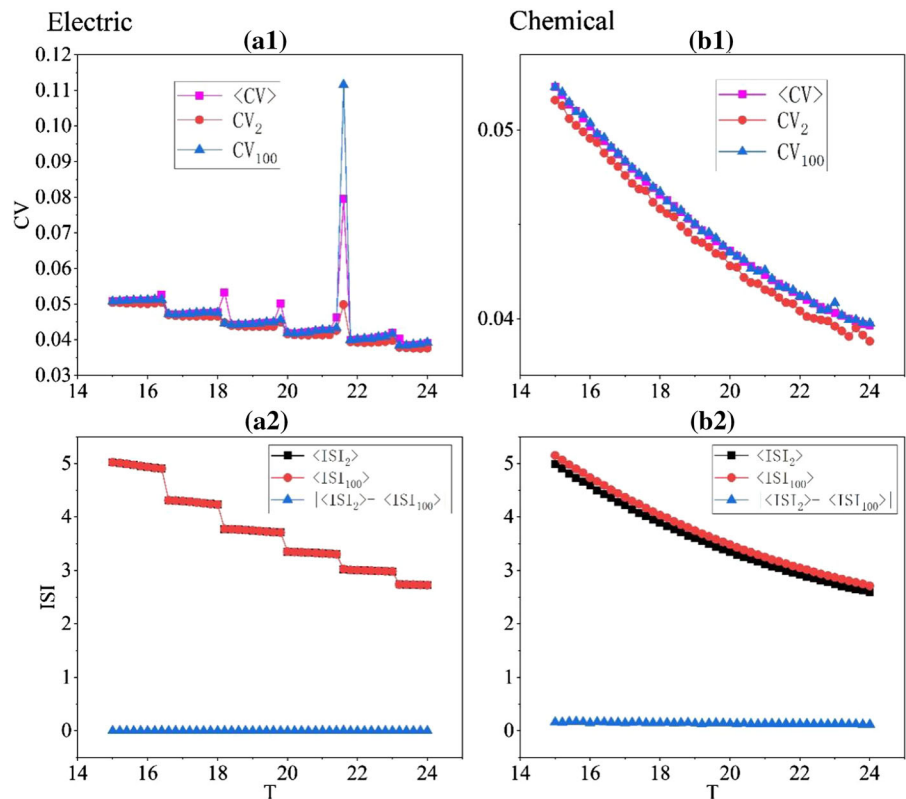
Fig. 13 Distribution of synchronization factors with increasing temperature for networks of different scales connected by chemical and electrical synapses when the time delay is fixed at $\tau = 20ms$ and the coupling intensity is $G = 0.1$. The effect of network scale on networks connected by both types is very small
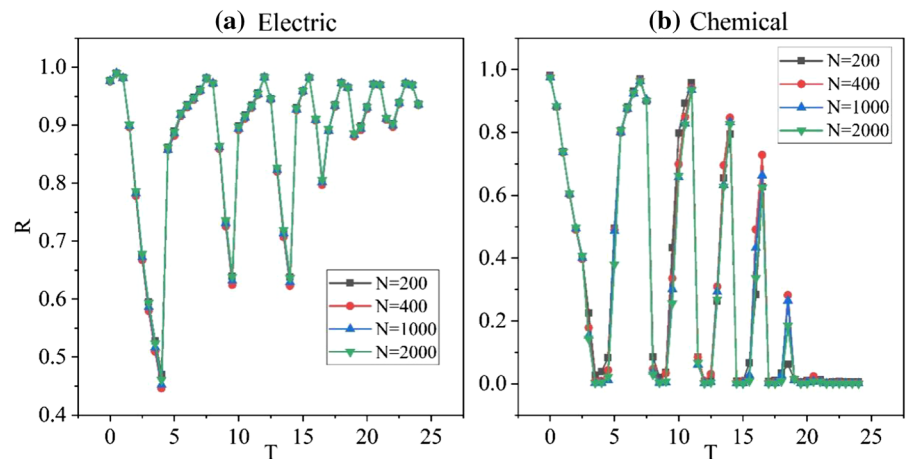
Finally, in order to determine whether the previously studied phenomena and their mechanisms in this paper are universal, the distribution of the synchronization factor with temperature is investigated in networks of different scales (with different number of nodes). It is found that the distribution of the synchronization factor with temperature change is not affected by the scale of the network in the role of time delay. This consequence proves the generality of our study.

Data availability All data generated or analyzed during this study are included in this published article.

Declarations

Conflict of interest The authors declare that they have no potential conflict of interest.

References

1. Hodgkin, A.L., Huxley, A.F.: A quantitative description of membrane current and its application to conduction and excitation in nerve. J. Physiol. **117**, 500–544 (1952)
2. Lu, L., Jia, Y., Kirunda, J.B., et al.: Effects of noise and synaptic weight on propagation of subthreshold excitatory postsynaptic current signal in a feed-forward neural network. Nonlinear Dyn. **95**, 1673–1686 (2018)
3. He, Z., Yao, C., Liu, S., et al.: Transmission of pacemaker signal in a small world neuronal networks: temperature effects. Nonlinear Dyn. **106**, 2547–2557 (2021)
4. Zhou, X., Xu, Y., Wang, G., et al.: Ionic channel blockage in stochastic Hodgkin-Huxley neuronal model driven by multiple oscillatory signals. Cogn. Neurodyn. **14**, 569–578 (2020)
5. Hindmarsh, J.L., Rose, R.M.: A model of neuronal bursting using three coupled first order differential equations. Proc. R. Soc. Lond. Ser. B **221**, 87–102 (1984)
6. FitzHugh, R.: Impulses and physiological states in theoretical models of nerve membrane. Biophys. J. **1**, 445–466 (1961)
7. Morris, C., Lecar, H.: Voltage oscillations in the barnacle giant muscle fiber. Biophys. J. **35**, 193–213 (1981)
8. Nagumo, J., Sato, S.: On a response characteristic of a mathematical neuron model. Kybernetik **10**, 155–164 (1972)
9. Wang, G., Yang, L., Zhan, X., et al.: Chaotic resonance in Izhikevich neural network motifs under electromagnetic induction. Nonlinear Dyn. **107**, 3945–3962 (2022)
10. Sathiyadevi, K., Premraj, D., Banerjee, T., et al.: Aging transition under discrete time-dependent coupling: restoring rhythmicity from aging. Chaos Soliton Fract. **157**, 111944 (2022)
11. Yu, D., Wang, G., Li, T., et al.: Filtering properties of Hodgkin-Huxley neuron on different time-scale signals. Commun. Nonlinear. Sci. (2022). https://doi.org/10.1016/j.cnsns.2022.106894
12. Ding, Q.M., Jia, Y.: Effects of temperature and ion channel blocks on propagation of action potential in myelinated axons. Chaos **31**, 053102 (2021)
13. Pereda, A.E.: Electrical synapses and their functional interactions with chemical synapses. Nat. Rev. Neurosci. **15**, 250–263 (2014)
14. Ge, M., Lu, L., Xu, Y., et al.: Vibrational mono-/bi-resonance and wave propagation in FitzHugh–Nagumo neural systems under electromagnetic induction. Chaos Soliton Fract. **133**, 109645 (2020)
15. Pouzat, C., Marty, A.: Autaptic inhibitory currents recorded from interneurones in rat cerebellar slices. J. Physiol. **509**, 777–783 (1998)
16. Bard Ermentrout, G., Terman, D.H.: Mathematical Foundations of Neuroscience. Springer, Berlin (2010)
17. Goto, A., Bota, A., Miya, K., et al.: Stepwise synaptic plasticity event drive the early phase of memory consolidation. Science **374**, 857–863 (2021)
18. Yin, L., Zheng, R., Ke, W., et al.: Autapses enchance bursting and coincidence detection in neocortical pyramidal cells. Nat. Commun. **9**, 4890 (2018)
19. Andreev, A.V., Frolov, N.S., Pisarchik, A.N., et al.: Chimera state in complex networks of bistable Hodgkin-Huxley neurons. Phys. Rev. E **100**, 022224 (2019)
20. Hay, E., Hill, S., Schürmann, F., et al.: Models of neocortical layer 5b pyramidal cells capturing a wide range of dendritic and perisomatic active properties. PLoS. Comput. Biol. **7**, e1002107 (2011)
21. Bono, J., Clopath, C.: Modeling somatic and dendritic spike mediated plasticity at the single neuron and network level. Nat. Commun. **8**, 706 (2017)
22. Fan, Y., Wei, X., Yi, G., et al.: Effects of hyperpolarization-active cation current (I_h) on sublinear dendritic integration under applied electric fields. Nonlinear Dyn. **108**, 4335–4356 (2022)
23. Hussain, I., Jafari, S., Ghosh, D., et al.: Synchronization and chimeras in a network of photosensitive FitzHugh–Nagumo neurons. Nonlinear Dyn. **104**, 2711–2721 (2021)
24. Xu, Y., Jia, Y., Ge, M., et al.: Effects of ion channel blocks on electrical activity of stochastic Hodgkin-Huxley neural network under electromagnetic induction. Neurocomputing **283**, 196–204 (2018)
25. Parastesh, F., Azarnoush, H., Jafari, S., et al.: Synchronizability of two neurons with switching in the coupling. Appl. Math. Comput. **350**, 217–223 (2019)
26. Wang, G., Yu, D., Ding, Q., et al.: Effects of electric field on multiple vibrational resonances in Hindmarsh-Rose neuronal systems. Chaos Soliton Fract. **150**, 111210 (2021)
27. Wu, Y., Wang, B., Zhang, X., et al.: Spiral wave of a two-layer coupling neuronal network with multi-area channels. Int. J. Mod. Phys. B **33**, 1950354 (2019)
28. Andreev, A.V., Maksimenko, V.A., Pisarchik, A.N., et al.: Synchronization of interacted spiking neuronal networks with inhibitory coupling. Chaos Soliton Fract. **146**, 110812 (2021)
29. Sathiyadevi, K., Chandrasekar, V.K., Senthilkumar, D.V.: Inhomogeneous to homogeneous dynamical states through symmetry breaking dynamics. Nonlinear Dyn. **98**, 327–340 (2019)
30. Barabási, A.-L., Albert, R.: Emergence of scaling in random networks. Science **286**, 509–512 (1999)
31. Watts, D.J., Strogatz, S.H.: Collective dynamics of small-world networks. Nature **393**, 440–442 (1998)
32. Wainrib, G., Touboul, J.: Topological and dynamical complexity of random neural networks. Phys. Rev. Lett. **110**, 118101 (2012)
33. Guo, L., Zhang, S., Wu, Y., et al.: Complex spiking neural networks with synaptic time-delay based on anti-

interference function. Cogn. Neurodyn. (2022). https://doi.org/10.1007/s11571-022-09803-4

34. Holstein, D., Goltsev, A.V., Mendes, J.: Impact of noise and damage on collective dynamics of scale-free neuronal networks. Phys. Rev. E **87**, 032717 (2013)

35. Ribeiro, T.L., Chialvo, D.R., Plenz, D.: Scale-free dynamics in animal groups and brain networks. Front. Syst. Neurosci. **14**, 591210 (2021)

36. Wang, Q., Perc, M., Duan, Z., et al.: Synchronization transitions on scale-free neuronal networks due to finite information transmission delays. Phys. Rev. E **80**, 026206 (2009)

37. Hao, Y., Gong, Y., Wang, L., et al.: Single or multiple synchronization transitions in scale-free neuronal networks with electrical or chemical coupling. Chaos Soliton Fract. **44**, 260–268 (2011)

38. Kundu, S., Bera, B.K., Ghosh, D., et al.: Chimera patterns in three-dimensional locally coupled systems. Phys. Rev. E **99**, 022204 (2019)

39. Yu, D., Wang, G., Ding, Q., et al.: Effects of bounded noise and time delay on signal transmission in excitable neural networks. Chaos Soliton Fract. **157**, 111929 (2022)

40. Rajagopal, K., Panahi, S., Chen, M., et al.: Suppressing spiral wave turbulence in a simple fractional-order discrete neuron map using impulse triggering. Fractals **29**, 2140030 (2021)

41. Paul Asir, M., Sathiyadevi, K., Philominathan, P., et al.: A nonlinear memductance induced intermittent and anti-phase synchronization. Chaos **32**, 073125 (2022)

42. Deco, G., Buehlmann, A., Masquelier, T., et al.: The role of rhythmic neural synchronization in rest and task conditions. Front. Hum. Neurosci. **5**, 4 (2011)

43. Li, T., Wang, G., Yu, D., et al.: Synchronization mode transitions induced by chaos in modified Morris-Lecar neural systems with weak coupling. Nonlinear Dyn. **108**, 2611–2625 (2022)

44. Yu, D., Lu, L., Wang, G., et al.: Synchronization mode transition induced by bounded noise in multiple time-delays coupled FitzHugh-Nagumo model. Chaos Soliton Fract. **147**, 111000 (2021)

45. Mehrabbeik, M., Parastesh, F., Ramadoss, J., et al.: Synchronization and chimera states in the network of electrochemically coupled memristive Rulkov neuron maps. Math. Biosci. Eng. **18**, 9394–9409 (2021)

46. Ramakrishnan, B., Parastesh, F., Jafari, S., et al.: Synchronization in a multiplex network of nonidentical fractional-order neurons. Fractal Fract. **6**, 169 (2022)

47. Steriade, M., McCormick, D.A., Sejnowski, J.: Thalamocortical oscillations in the sleeping and aroused brain. Science **262**, 5134 (1993)

48. Knoblich, U., Huang, L., Zeng, H., et al.: Neuronal cell-subtype specificity of neural synchronization in mouse primary visual cortex. Nat. Commun. **10**, 2533 (2019)

49. Fell, J., Axmacher, N.: The role of phase synchronization in memory processes. Nat. Rev. Neurosci. **12**, 105–114 (2011)

50. Gaillard, R., Dehaene, S., Adam, C., et al.: Converging intracranial markers of conscious access. PLoS Biol. **7**, e1000061 (2009)

51. Roelfsema, P.R., Engel, A.K., König, P., et al.: Visuomotor integration is associated with zero time-lag synchronization among cortical areas. Nature **385**, 157–161 (1997)

52. Rodriguez, E., George, N., Lachaux, J.-P., et al.: Varela, perception's shadow: long-distance synchronization of human brain activity. Nature **397**, 430–433 (1999)

53. Mormann, F., Lehnertz, K., David, P., et al.: Mean phase coherence as a measure for phase synchronization and its application to the EEG of epilepsy patients. Phys. D **144**, 358–369 (2000)

54. Galvan, A., Wichmann, T.: Pathophysiology of parkinsonism. Clin. Neurophysiol. **119**, 1459–1474 (2008)

55. Lee, D.S.: Synchronization transition in scale-free networks: clusters of synchrony. Phys. Rev. E **72**, 026208 (2005)

56. Sorrentino, F., di Bernardo, M., Huerta Cuéllar, G., et al.: Synchronization in weighted scale-free networks with degree-degree correlation. Physica D **224**, 123–129 (2006)

57. Budzinski, R.C., Rossi, K.L., Boaretto, B.R.R., et al.: Synchronization malleability in neural networks under a distance-dependent coupling. Phys. Rev. R. **2**, 043309 (2020)

58. Yu, Y., Hill, A.P., McCormick, D.A.: Warm body temperature facilitates energy efficient cortical action potentials. PLoS Comput. Biol. **8**, e1002456 (2012)

59. Rowbury, R.J.: Temperature effects on biological systems: introduction. Sc. Prog. **86**, 1–7 (2003)

60. Arcus, V.L., Prentice, E.J., Hobbs, J.K., et al.: On the temperature dependence of enzyme-catalyzed rates. Biochemistry **55**, 1681–1688 (2016)

61. Fu, X., Yu, Y.G.: Reliable and efficient processing of sensory information at body temperature by rodent cortical neurons. Nonlinear Dyn. **98**, 215–231 (2019)

62. Song, X.L., Wang, H.T., Chen, Y., et al.: Emergence of an optimal temperature in action-potential propagation through myelinated axons. Phys. Rev. E **100**, 032416 (2019)

63. Wang, G., Wu, Y., Xiao, F., et al.: Non-Gaussian noise and autapse-induced inverse stochastic resonance in bistable Izhikevich neural system under electromagnetic induction. Physica A **598**, 127274 (2022)

64. Ochab-Marcinek, A., Schmid, G., Goychuk, I., et al.: Noise-assisted spike propagation in myelinated neurons. Phys. Rev. E **79**, 011904 (2009)

65. Ge, M., Wang, G., Jia, Y.: Influence of the Gaussian colored noise and electromagnetic radiation on the propagation of subthreshold signals in feedforward neural networks. Sci. China Tech. Sci. **64**, 847–857 (2021)

66. Premraj, D., Suresh, K., Banerjee, T., et al.: Bifurcation delay in a network of locally coupled slow-fast systems. Phys. Rev. E **98**, 022206 (2018)

67. Machado, J.N., Matias, F.S.: Phase bistability between anticipated and delayed synchronization in neuronal populations. Phys. Rev. E **102**, 032412 (2020)

68. Lu, L., Yang, L., Zhan, X., et al.: Cluster synchronization and firing rate oscillation induced by time delay in random network of adaptive exponential integrate-and-fire neural system. Eur. Phys. J. B **93**, 205 (2020)

69. Wang, Q., Perc, M., Duan, Z., et al.: Delay-enhanced coherence of spiral waves in noisy Hodgkin-Huxley neuronal networks. Phys. Lett. A **372**, 5681–5687 (2008)

70. Sainz-Trapága, M., Masoller, C., Braun, H.A., et al.: Influence of time-delayed feedback in the firing pattern of thermally sensitive neurons. Phys. Rev. E **70**, 031904 (2004)

71. Guo, Y., Zhou, P., Yao, Z., et al.: Biophysical mechanism of signal encoding in an auditory neuron. Nonlinear Dyn. **105**, 3603–3614 (2021)

72. Wang, H., Chen, Y.: Spatiotemporal activities of neural network exposed to external electric fields. Nonlinear Dyn. **85**, 881–891 (2016)

73. Lu, L., Kirunda, J.B., Xu, Y., et al.: Effects of temperature and electromagnetic induction on action potential of Hodgkin-Huxley model. Eur. Phys. J-Spec. Top. **227**, 767–776 (2018)

74. Rall, W.: Distinguishing theoretical synaptic potentials computed for different soma-dendritic distributions of synaptic inputs. J. Ncurophysiol. **30**, 1138–1168 (1967)

75. Gonze, D., Bernard, S., Waltermann, C., et al.: Spontaneous synchronization of coupled circadian oscillators. Biophys. J. **89**, 120–129 (2005)

76. Schmid, G., Goychuk, I., Hänggi, P.: Stochastic resonance as a collective property of ion channel assemblies. Europhys. Lett. **56**, 22–28 (2001)